

# Synthesis, structure, spectra and reactivity of iron(III) complexes of imidazole and pyrazole containing ligands as functional models for catechol dioxygenases†

Thirumanasekaran Dhanalakshmi,<sup>a</sup> Eringathodi Suresh<sup>b</sup> and Mallayan Palaniandavar<sup>\*a</sup>

Received 20th February 2009, Accepted 15th July 2009

First published as an Advance Article on the web 17th August 2009

DOI: 10.1039/b903602d

A series of new 1 : 1 iron(III) complexes of the type [Fe(L)Cl<sub>3</sub>], where L is a tridentate 3N donor ligand, has been isolated and studied as functional models for catechol dioxygenases. The ligands (1-methyl-1*H*-imidazol-2-ylmethyl)pyrid-2-ylmethyl-amine (**L1**), *N,N*-dimethyl-*N'*-(1-methyl-1*H*-imidazol-2-ylmethyl)ethane-1,2-diamine (**L2**) and *N*-(1-methyl-1*H*-imidazol-2-ylmethyl)-*N'*-phenylethane-1,2-diamine (**L3**) are linear while the ligands tris(1-pyrazolyl)methane (**L4**), tris(3,5-dimethyl-1-pyrazolyl)methane (**L5**) and tris(3-*iso*-propylpyrazolyl)methane (**L6**) are tripodal ones. All the complexes have been characterized by spectral and electrochemical methods. The X-ray crystal structure of the dinuclear catecholate adduct [Fe(**L2**)(TCC)]<sub>2</sub>O, where TCC<sup>2-</sup> is a tetrachlorocatecholate dianion, has been successfully determined. In this complex both the iron(III) atoms are bridged by a μ-oxo group and each iron(III) center possesses a distorted octahedral coordination geometry in which the ligand **L2** is facially coordinated and the remaining coordination sites are occupied by the TCC<sup>2-</sup> dianion. Spectral studies suggest that addition of a base like Et<sub>3</sub>N induces the mononuclear complex species [Fe(**L2**)(TCC)Cl] to dimerize forming a μ-oxo-bridged complex. The spectral and electrochemical properties of the catecholate adducts of the complexes generated *in situ* reveal that a systematic variation in the ligand donor atom type significantly influences the Lewis acidity of the iron(III) center and hence the interaction of the complexes with simple and substituted catechols. The 3,5-di-*tert*-butylcatecholate (DBC<sup>2-</sup>) adducts of the type [Fe(L)(DBC)Cl], where L is a linear tridentate ligand (**L1**–**L3**), undergo mainly oxidative intradiol cleavage of the catechol in the presence of dioxygen. Also, the extradiol-to-intradiol product selectivity (E : I) is enhanced upon removal of the coordinated chloride ion in these adducts to obtain [Fe(L)(DBC)(Sol)]<sup>+</sup> and upon incorporating coordinated *N*-methylimidazolyl nitrogen in them. In contrast to the iron(III) complexes of imidazole-based ligands, those of the tripodal pyrazole-based ligands **L4**–**L6** yield major amounts of the oxidized product benzoquinone and small amounts of both intra- and extradiol products. One of the pyrazole arms coordinated in the equatorial plane of these sterically constrained complexes is substituted by a solvent molecule upon adduct formation with DBC<sup>2-</sup>, which encourages molecular oxygen to attack this site leading to benzoquinone formation. The DBSQ/DBC<sup>2-</sup> redox potentials of both the imidazole- and pyrazole-based complexes fall in the narrow range of –0.186 to –0.214 V supporting this proposal.

## Introduction

The catechol dioxygenases are mononuclear non-heme iron enzymes isolated from soil bacteria.<sup>1,2</sup> They have attracted much interest because they convert aromatic pollutants in the environment to water-soluble aliphatic products by oxidative ring cleavage<sup>3,4</sup> with the incorporation of both atoms of dioxygen into the aromatic ring. They are subdivided into intradiol- and extradiol-cleaving enzymes depending on the catalysis of ring cleavage between or outside the two *ortho*-hydroxyl groups.<sup>5</sup> The intradiol-cleaving

enzymes exemplified by catechol 1,2-dioxygenase (CTD) and protocatechuate 3,4-dioxygenase (3,4-PCD) possess a high-spin iron(III) center<sup>6</sup> bound to the protein backbone primarily by two histidine imidazole nitrogen and two phenolate oxygen (tyrosinate) atoms in a five-coordinate trigonal bipyramidal geometry.<sup>7,8</sup> In contrast, the extradiol dioxygenases utilize an iron(II) cofactor ligated by two histidine nitrogens and one glutamic acid in a square-pyramidal geometry.<sup>9</sup>

Several bioinorganic modeling studies<sup>10–21</sup> have focused on the structural and spectroscopic characterization of iron(III) complexes of linear<sup>11,12,20</sup> and tripodal tetradentate<sup>14–16,19,20</sup> and tetraaza macrocyclic<sup>17,18</sup> ligands as structural and functional models for the catecholate-iron(III) form of catechol dioxygenases. In a vast majority of these studies the oxygenation products reported are consistent with intradiol cleavage. The significance of Lewis acidity of iron(III) center in the dioxygenase reaction has been highlighted<sup>10–14</sup> and a substrate activation mechanism has been postulated for

<sup>a</sup>School of Chemistry, Bharathidasan University, Tiruchirappalli, 620 024, India. E-mail: palanim51@yahoo.com, palaniandavarm@gmail.com; Tel: +91-431-2407125

<sup>b</sup>Analytical Science Discipline, Central Salt and Marine Chemicals Research Institute, Bhavnagar, 364 002, India

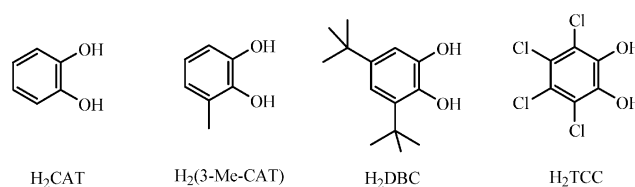
† CCDC reference number 721218. For crystallographic data in CIF or other electronic format see DOI: 10.1039/b903602d

intradiol-cleaving enzymes.<sup>5,6</sup> In contrast, model complexes that elicit extradiol cleavage activity are fewer in number<sup>22–34</sup> and a five-coordinate iron center as in the active sites of the extradiol-cleaving enzymes has been suggested<sup>9</sup> to be necessary for the extradiol cleavage to occur. Also, the model complexes so far reported have emphasized the importance of facial coordination of tridentate ligands and a vacant coordination position for oxygen binding as well in order to elicit extradiol cleavage.<sup>25–28</sup> Thus, iron(III) complexes of meridionally coordinating tridentate ligands like terpyridine yield quinone in a large amount and intradiol cleavage products, while those of facially coordinating macrocyclic 3N ligands like triazacyclononane (tacn), 1,4,7-trimethyl-1,4,7-triazacyclononane (Me<sub>3</sub>TACN), and *N*-benzyl-*N,N'*-bis(2-pyridylmethyl)amine elicit extradiol cleavage.<sup>28</sup> In our laboratory, several mononuclear iron(III) complexes of tridentate 3N<sup>21,30,31</sup> and 2NO<sup>14,21</sup> and tetradentate 4N<sup>14,34</sup> and 3NO<sup>14,20,33</sup> ligands have been studied as functional models for catechol dioxygenases. Gebbink *et al.* have isolated the catecholate adducts of iron(II) and iron(III) complexes of a new family of substituted 3,3-bis(1-alkylimidazol-2-yl)propionate ligands, which elicit both the extradiol and intradiol cleavage products in comparable amounts.<sup>32</sup>

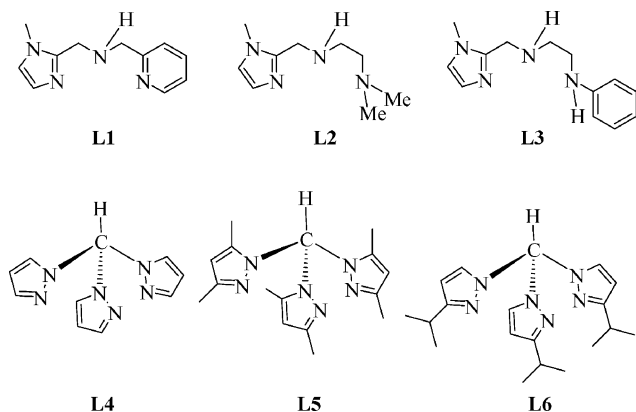
From our laboratory we have reported<sup>31</sup> iron(III) complexes of linear tridentate *N*-alkyl substituted bis(pyrid-2-ylmethyl)amine (BPA) ligands as models for extradiol-cleaving enzymes. The nature of the *N*-alkyl substituents in these complexes controls the regioselectivity of catechol cleavage and enhances the extradiol cleavage yield to 46–68% in dichloromethane. Very recently, we also found<sup>30</sup> that the iron(III) complexes with both centrally and terminally *N*-alkyl substituted (pyrid-2-ylmethyl)ethylenediamine 3N ligands exhibit higher extradiol-to-intradiol product selectivity in dichloromethane solvent. As the imidazole group of the histidine amino acid acts as the nitrogen donor in the enzyme active sites, we have now become interested in the study of 1 : 1 iron(III) complexes of imidazole-containing linear ligands (**L1–L3**, Scheme 1) as models for catechol dioxygenase enzymes and the effect of the imidazolyl moiety on the dioxygenase activity of the iron(III) complexes has been probed. Indeed, it is remarkable that the *N*-Me-imidazolyl moiety in the iron(III) complex of a tripodal tetradentate monophenolate ligand enhances the reaction rate with efficient conversion (77.1%) of the substrate to intradiol cleavage products.<sup>20</sup> Incorporation of *N*-alkyl substituents on the terminal amine nitrogen atom in the iron(III) complexes<sup>30</sup> of (pyrid-2-ylmethyl)ethylenediamine ligands leads to confer ex-

tradiol cleavage with yields relatively higher than those on the central nitrogen atom in the BPA-based complexes.<sup>31</sup> The effect of varying the steric bulk of the terminal donor group in the present imidazolyl-based ligands has been studied. The results indicate that mainly intradiol cleavage products are obtained but with the extradiol-to-intradiol product selectivity being lower than those for the corresponding pyridyl-based complexes.<sup>21</sup> The dinuclear  $\mu$ -oxo-bridged tetrachlorocatecholate adduct of one of the complexes of the imidazolyl-based ligands has been structurally characterized to show the ability of these ligands to engage in facial coordination.

Also, Moro-Oka *et al.*<sup>27</sup> have reported the iron(III) complexes of the sterically hindered tris(pyrazolyl)borate ligands hydrotris(3-*tert*-butyl-5-*iso*-propyl-1-pyrazolyl)borate (Tp<sup>Bu,Pr</sup>) and hydrotris(3,5-di-*iso*-propyl-1-pyrazolyl)borate (Tp<sup>Pr<sub>2</sub></sup>) as structural and functional models for the catechol dioxygenases and found that the complex with the ligand Tp<sup>Pr<sub>2</sub></sup> alone reacts with O<sub>2</sub> to cause extradiol cleavage. In continuation of our work<sup>30,31</sup> to explore the necessity of facial coordination of ligands to elicit extradiol cleavage, simple tripodal tridentate tris(pyrazolyl)methane ligands with different substituents (**L4–L6**, Scheme 1) have also been used, and the reactivity of iron(III) complexes of these ligands towards cleavage of H<sub>2</sub>DBC has been investigated. Also, it is expected that the differently substituted pyrazoles in the ligands **L4–L6** would impose varying steric and electronic effects on the iron(III) coordination geometry, tune the Lewis acidity of the iron(III) center and hence affect the dioxygenase activity of the complexes. Interestingly, all the pyrazolyl-based complexes yield the oxidized product benzoquinone in major amounts and both intra- and extradiol cleavage products in smaller amounts. The interaction of all the present complexes with a series of catechols (Scheme 2) has been monitored using electronic absorption spectral and electrochemical methods.



Scheme 2 Structures of catechols used.



Scheme 1 Structures of ligands used.

## Results and discussion

### Syntheses of ligands and iron(III) complexes

The linear tridentate ligands **L1–L3** were synthesized by the condensation of 1-methylimidazole-2-carboxaldehyde with the corresponding amines to form a Schiff base followed by the reduction of the latter with sodium borohydride.<sup>21,30</sup> The ligands **L4–L6** were synthesized according to known procedures,<sup>35,36</sup> which involve the treatment of chloroform with the corresponding pyrazole in the presence of sodium carbonate and a phase transfer catalyst like tetra-*n*-butylammonium bromide. They were reacted with equimolar amounts of iron(III) chloride in methanol to obtain mononuclear 1 : 1 iron(III) complexes. The differently substituted amine functions in the ligands are expected to impose steric and electronic effects on the iron(III) coordination geometry, tune the

Lewis acidity of the iron(III) center and hence determine the dioxygenase activity of the complexes. On the basis of the results of elemental analyses the present iron(III) complexes are formulated as  $[\text{Fe}(\text{LCl}_3)]$ , which is supported by the ESI-MS data. Conductivity studies of the 1:1 complexes in DMF solution ( $\Lambda_{\text{M}}$ , 290–320  $\text{ohm}^{-1} \text{cm}^2 \text{mol}^{-1}$ ) reveal that solvent molecules replace all the three coordinated chloride ions. This suggests that the bidentate catechols would bind to the coordination positions occupied by chloride ions. The present iron(III) complexes **1–6** have magnetic moments in the range 5.95–6.05 BM at room temperature, which is characteristic of a high-spin iron(III) center.

### Description of the structure of $[(\text{Fe}(\text{L}2)(\text{TCC}))_2\text{O}]\cdot 2(\text{CH}_3)_2\text{CO}\cdot\text{H}_2\text{O} **7**$

An ORTEP view of the molecular structure of complex **7** including the atom numbering scheme is given in Fig. 1 (crystal data and structure refinement details can be found in Table 1). Selected bond distances and bond angles relevant to the iron coordination sphere are listed in Table 2. The unit cell contains one dinuclear iron(III) complex with a  $\mu$ -oxo bridge and also one water and two acetone molecules of crystallization. The coordination sphere of each iron(III) center has a distorted octahedral geometry. Since the bridging oxygen atom O(3) is located on the centre of symmetry, the second half of the dinuclear complex is generated by inversion of the first. The  $\text{Fe}\cdots\text{Fe}$  distance is 3.5612 Å and both the iron atoms are surrounded by a  $\text{N}_3\text{O}_3$  donor set, each constituted by the three nitrogen (N1, N3, N4) atoms of the facially coordinated ligand **L2**, two oxygen atoms (O1, O3) of the dianionic tetrachlorocatecholate and one oxygen atom of the  $\mu$ -oxo bridge. The facial coordination of **L2** is similar to that of the 3 N ligands in mononuclear octahedral iron(III) complexes.<sup>28,30</sup> The  $\text{Fe}-\text{N}_{\text{amine}}$  bonds ( $\text{Fe}-\text{N}3$ , 2.337(5);  $\text{Fe}-\text{N}4$ , 2.232(4) Å) are longer than the  $\text{Fe}-\text{N}_{\text{im}}$  bond (2.117(3)Å) due to  $\text{sp}^3$  and  $\text{sp}^2$  hybridization respectively of the amine and imidazole nitrogen

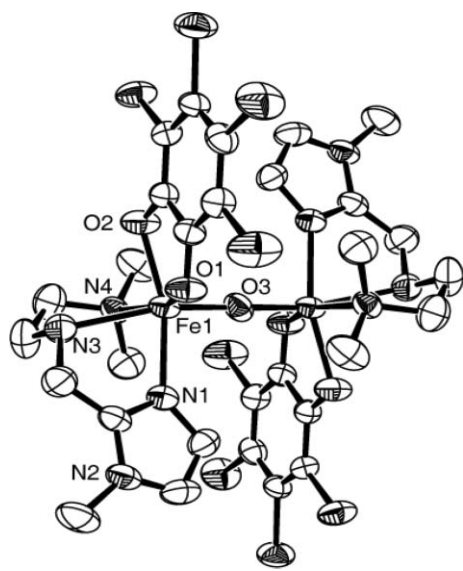


**Fig. 1** ORTEP diagram of complex **7** showing 50% probability thermal ellipsoids and the labelling scheme for selected atoms. All hydrogen atoms are omitted for clarity. The symmetry operation  $2 - x, 1 - y, -z$  is used to generate  $\text{Fe}(1_{\text{a}})$ .

**Table 1** Crystal data and structure refinement details for **7**

7	
Empirical formula	$\text{C}_{30}\text{H}_{34}\text{Cl}_6\text{Fe}_2\text{N}_8\text{O}_5 \cdot 2(\text{C}_3\text{H}_6\text{O}) \cdot \text{O}$
Formula weight	1114.12
Crystal system	Triclinic
Crystal size	$0.08 \times 0.14 \times 0.24$
Space group	$P\bar{1}$ (No. 2)
$a/\text{\AA}$	10.696(5)
$b/\text{\AA}$	10.942(5)
$c/\text{\AA}$	12.328(6)
$\alpha/^\circ$	89.689(8)
$\beta/^\circ$	75.395(8)
$\gamma/^\circ$	60.989(8)
$V/\text{\AA}^3$	1209.3(10)
$Z$	1
$\lambda(\text{Mo K}\alpha)/\text{\AA}$	0.71073
$D_{\text{calc}}/\text{g cm}^{-3}$	1.530
Temperature/K	293
Goodness-of-fit on $F^2$	0.99
Number of reflections measured	7160
Number of reflections used	5301
Number of L.S. restraints	0
Number of refined parameters	291
$R_{\text{(int)}}$	0.033
Final $R$ indices [ $I > 2\sigma(I)$ ]	
$R_1^a$	0.0634
$wR_2^b$	0.1601

<sup>a</sup>  $R_1 = [\sum(|F_o| - |F_c|)/\sum|F_o|]$ . <sup>b</sup>  $wR_2 = \{[\sum(w(F_o^2 - F_c^2)^2)/\sum(wF_o^4)]^{1/2}\}$ .

**Table 2** Selected bond lengths (Å) and angles (°) for **7**

Bond lengths		Bond angles	
$\text{Fe}(1)-\text{O}(1)$	2.035(4)	$\text{O}(1)-\text{Fe}(1)-\text{O}(2)$	80.57(12)
$\text{Fe}(1)-\text{O}(2)$	2.018(4)	$\text{O}(1)-\text{Fe}(1)-\text{O}(3)$	102.91(11)
$\text{Fe}(1)-\text{O}(3)$	1.7806(12)	$\text{O}(1)-\text{Fe}(1)-\text{N}(1)$	90.10(13)
$\text{Fe}(1)-\text{N}(1)$	2.117(3)	$\text{O}(1)-\text{Fe}(1)-\text{N}(3)$	88.52(14)
$\text{Fe}(1)-\text{N}(3)$	2.337(5)	$\text{O}(1)-\text{Fe}(1)-\text{N}(4)$	161.02(16)
$\text{Fe}(1)-\text{N}(4)$	2.232(4)	$\text{O}(2)-\text{Fe}(1)-\text{O}(3)$	104.28(12)
		$\text{O}(2)-\text{Fe}(1)-\text{N}(1)$	159.36(18)
		$\text{O}(2)-\text{Fe}(1)-\text{N}(3)$	87.44(15)
		$\text{O}(2)-\text{Fe}(1)-\text{N}(4)$	86.37(13)
		$\text{O}(3)-\text{Fe}(1)-\text{N}(1)$	95.71(13)
		$\text{O}(3)-\text{Fe}(1)-\text{N}(3)$	164.70(11)
		$\text{O}(3)-\text{Fe}(1)-\text{N}(4)$	93.60(13)
		$\text{N}(1)-\text{Fe}(1)-\text{N}(3)$	73.86(16)
		$\text{N}(1)-\text{Fe}(1)-\text{N}(4)$	97.61(14)
		$\text{N}(3)-\text{Fe}(1)-\text{N}(4)$	77.12(15)
		$\text{Fe}(1)-\text{O}(3)-\text{Fe}(1_{\text{a}})$	180.00

The symmetry operation that generates  $\text{Fe}(1_{\text{a}})$  is  $2 - x, 1 - y, -z$ .

atoms. The  $\text{Fe}-\text{N}3_{\text{amine}}$  bond is longer than the  $\text{Fe}-\text{N}4_{\text{amine}}$  bond due to the strong *trans* effect imposed by the  $\mu$ -oxo bridge leading to the lengthening of  $\text{Fe}(1)-\text{N}(3)$  bond and hence the stronger binding of the other two nitrogen atoms (N1 and N4). Consequently, the  $\text{Fe}-\text{O}_{\text{cat}}$  bonds [ $\text{Fe}-\text{O}1$ , 2.035(4);  $\text{Fe}-\text{O}2$ , 2.018(4) Å] *trans* to the nitrogen atoms also become different in length and are longer than those in the  $\text{TCC}^{2-}$  adducts of iron(III) complexes of tri-<sup>27,28,31,32</sup> and tetradentate<sup>16,34,37,38</sup> ligands. The structure is similar to that of the complex<sup>37</sup>  $[(\text{Fe}(\text{L}7)(\text{tcc}))_2\text{O}]$  **8**, where **L7** is the tridentate ligand *N'*-acetyl-*N,N*-bis[(2-pyridyl)methyl]ethylenediamine, and the  $\text{Fe}(1)-\text{O}(3)$  bond (1.7806(12) Å) is shorter than that in **8** (1.7929(5) Å) suggesting the presence of a higher negative charge

**Table 3** Electronic spectral data ( $\lambda_{\text{max}}$  in nm;  $\epsilon_{\text{max}}$  in  $\text{M}^{-1} \text{cm}^{-1}$  in parenthesis) for iron(III) complexes<sup>a</sup> and their adducts in dimethylformamide solution

Added ligand <sup>b</sup>	$\lambda_{\text{max}}/\text{nm}$ ( $\epsilon$ , $\text{M}^{-1}\text{cm}^{-1}$ )					
	[Fe(L1)Cl <sub>3</sub> ]	[Fe(L2)Cl <sub>3</sub> ]	[Fe(L3)Cl <sub>3</sub> ]	[Fe(L4)Cl <sub>3</sub> ]	[Fe(L5)Cl <sub>3</sub> ]	[Fe(L6)Cl <sub>3</sub> ]
None	325 sh	310 (2430)	301 (6930)	342 (2730)	328 (3490)	336 (2570)
	275 (11 332)	260 (5850)	267 (6570)	280 (74 100)	276 (72 570)	272 (78 260)
DBC <sup>2-c</sup>	795 (2505)	780 (1920)	718 (1598)	660 (1710)	655 (1670)	670 (1920)
	490 (1730)	485 (1575)	503 (1590)	530 (1390)	528 (1390)	546 (1620)
3-MeCAT <sup>2-c</sup>	765 (2490)	750 (1935)	697 (1396)	625 (1900)	605 (1770)	625 (1940)
	480 (1805)	475 (1625)	467 (1474)	502 (1560)	510 (1645)	490 (1590)
CAT <sup>2-c</sup>	745 (2490)	735 (2010)	710 (1546)	600 (1700)	585 (1645)	600 (1740)
	455 (1770)	445 (1670)	451 (1484)	450 (1520)	—	440 (1610)
TCC <sup>2-c</sup>	677 (2252)	665 (2075)	620 (1908)	590 (1821)	588 (1950)	596 (1990)
	455 (1585)	450 (1530)	434 (1379)	—	—	—

<sup>a</sup> Concentration of iron(III) complexes,  $2 \times 10^{-4}$  M. <sup>b</sup> The ratio of added ligand to iron(III) complexes was 1:1; the anions were generated by adding 2 equivalents of triethylamine. <sup>c</sup> H<sub>2</sub>DBC = 3,5-di-*tert*-butylcatechol; H<sub>2</sub>-3-MeCAT = 3-methylcatechol; H<sub>2</sub>CAT = catechol; H<sub>2</sub>TCC = 3,4,5,6-tetrachlorocatechol.

on the oxo group. Furthermore, the difference (0.017 Å) in Fe<sup>III</sup>-O<sub>cat</sub> bonds in **7** with dianionic catechol binding is much lower than that (0.2–0.4 Å) observed<sup>39</sup> in the Fe<sup>III</sup>-O<sub>cat</sub> bonds of BphC enzyme-substrate complex reflecting the monoanionic coordination of catechol in the latter.

### Electronic absorption spectra

The results obtained from the electronic absorption spectral studies on the iron(III) complexes and their adducts with different substituted catechols are provided in Table 3. While the spectral features observed in the range 300–375 nm may be assigned to Cl<sup>-</sup> → Fe(III) charge transfer transition,<sup>20</sup> the intense absorption band observed in the range 260–280 nm is ascribed to the  $\pi \rightarrow \pi^*$  transition within the imidazole moiety of the ligands. The interaction of the iron(III) complexes with a series of catechols were studied by using electronic spectroscopy to understand the electronic environment around iron(III) upon catecholate adduct formation. Two new visible bands (434–503 nm, 620–795 nm, Fig. 2) appear on adding catechols pre-treated with two equivalents of Et<sub>3</sub>N to the iron(III) complexes **1–6** in DMF solution. They are assignable to catecholate-to-iron(III) LMCT transitions involving two different catecholate ligand orbitals and  $d\pi^*$  orbital of iron(III).<sup>14,16</sup>

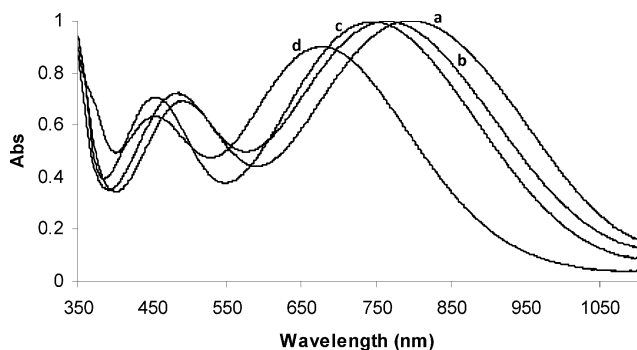


**Fig. 2** Electronic absorption spectra of adducts of complex **1** ( $4 \times 10^{-4}$  M) generated *in situ* by adding equimolar amounts of various catecholate dianions in DMF solution: [Fe(L1)(DBC)Cl] (a), [Fe(L1)(3-MeCAT)Cl] (b), [Fe(L1)(CAT)Cl] (c), [Fe(L1)(TCC)Cl] (d).

For the 3,5-di-*tert*-butylcatecholate (DBC<sup>2-</sup>) adducts [Fe(L)(DBC)Cl] generated in DMF both the low- and high-energy

LMCT bands exhibit remarkable dependence on the nature of the tridentate ligand<sup>11,17</sup> and the magnitude of energy of this band reflects the Lewis acidity of the iron(III) center as modified by the ligands. The LMCT band energies increase in the order: **1** < **2** < **3** and a similar variation in band energies are observed for the other catecholate adducts also. On replacing one of the pyridyl moieties<sup>31</sup> in [Fe(L8)(DBC)Cl], where **L8** is bis(pyrid-2-ylmethyl)amine, by *N*-methylimidazolyl group to obtain [Fe(L1)(DBC)Cl] and the pyridyl moiety<sup>30</sup> in [Fe(L9)(DBC)Cl], where **L9** is *N'*-(pyrid-2-ylmethyl)-*N,N*-dimethylethylenediamine, by *N*-Me-imidazolyl moiety to obtain [Fe(L2)(DBC)Cl], the catecholate-to-iron(III) LMCT bands are shifted to a higher energy. Incorporation of the electron-releasing *N*-Me-imidazolyl moiety destabilizes<sup>16,20</sup> the  $d\pi^*$  orbital on iron(III) leading to an increase in  $d\pi^*$ -catecholate orbital energy gap and hence a shift in the LMCT band to a higher energy. Also, interestingly, upon replacing the pyridylmethyl arm in [Fe(L1)(DBC)Cl] by the -CH<sub>2</sub>-NMe<sub>2</sub> and -CH<sub>2</sub>-NPh arms to get [Fe(L2)(DBC)Cl] and [Fe(L3)(DBC)Cl] respectively, the catecholate-to-iron(III) LMCT band is shifted to higher energies. It is clear that the electron-releasing effect rather than the steric bulk of -NMe<sub>2</sub> and -NPh groups is important in dictating the electronic environment around iron(III) in the catecholate adducts. Also, it is interesting that in DMF the low energy LMCT band of [Fe(L5)(DBC)Cl] is lower in energy than that of [Fe(L4)(DBC)Cl] while the low energy band of [Fe(L6)(DBC)Cl] is higher in energy than that of [Fe(L4)(DBC)Cl]. It is obvious that incorporation of the sterically demanding *iso*-propyl substituent in [Fe(L6)(DBC)Cl] would hinder the coordination of the pyrazole nitrogen and concomitantly stabilize the  $d\pi^*$  orbital leading to a decrease in  $d\pi^*$ -catecholate orbital energy gap and hence the shift in the LMCT band to low energy. On the other hand, incorporation of electron-releasing methyl groups on the pyrazole ring in [Fe(L5)(DBC)Cl] adduct would enhance the electron density on  $d\pi^*$  orbital and destabilize it leading to an increase in  $d\pi^*$ -catecholate orbital energy gap and hence the shift in the LMCT band to a higher energy. As both steric and electronic effects of the ligand donor atoms are significant in affecting the energies of the LMCT bands they should also affect the electronic environment around iron(III) and hence the dioxygenase activity of the complexes. It is interesting to note that the visible bands for the adducts [Fe(Tp<sup>(Bu,Pr)</sup>)(DBC)Cl] (672, 830 nm) and

[Fe(Tp<sup>iPr2</sup>)(DBC)Cl] (574, 1046 nm)<sup>27</sup> appear at wavelengths higher than the present complexes. The iron(III) center in these adducts of the anionic tris(pyrazolyl)borate ligands are more Lewis acidic than those of tris(pyrazolyl)methane ligands.

The position of the low energy catecholate → Fe(III) LMCT band depends also upon the substituents<sup>11</sup> on the catecholate ring. Thus the energy of the band is found to shift to higher energy as the substituents on the catecholate ring are varied from electron-donating to electron-withdrawing: H<sub>2</sub>DBC (795 nm) > H<sub>2</sub>3-MeCAT (765 nm) > H<sub>2</sub>CAT (745 nm) > H<sub>2</sub>TCC (677 nm) for complex **1**. A similar variation is also observed for other complexes. Electron-donating substituents would be expected to raise the energy of the catecholate frontier orbitals and thus minimize the ligand-to-metal energy gap. Thus the 3,5-di-*tert*-butylcatecholate (DBC<sup>2-</sup>) adducts of the iron(III) complexes absorb at energies lower than the other catecholate adducts. Similar spectral trends have been observed for the catecholate-bound iron(III) complexes of tridentate 3N<sup>21,30,31</sup> and tetradentate ligands.<sup>20</sup>

### Spectrophotometric titrations

The spectrophotometric titrations<sup>37</sup> were carried out to investigate the ability of **2** to form the μ-oxo bridged complex **7** and also to gain an insight into the species distribution in solution upon adding an external base to a mixture of the iron(III) complex and the substrate tetrachlorocatechol (H<sub>2</sub>TCC). To a 4 × 10<sup>-4</sup> M methanolic solution of complex **2** was added a 4 × 10<sup>-4</sup> M solution of H<sub>2</sub>TCC and the resulting mixture was titrated with a methanolic solution of piperidine (0.3 M) and the results are presented in Fig. 3. Similar results were obtained when Et<sub>3</sub>N was used as the base. Upon adding 0.0–0.5 equivalents of piperidine, the two catecholate-to-iron(III) LMCT bands appear around 475 and 745 nm and then rise in absorbance (1.0–2.0 equivalents of base) dramatically suggesting the formation of the mononuclear substrate adduct. Upon adding a further amount of base (3.0 equivalents), the two bands start disappearing and a new band

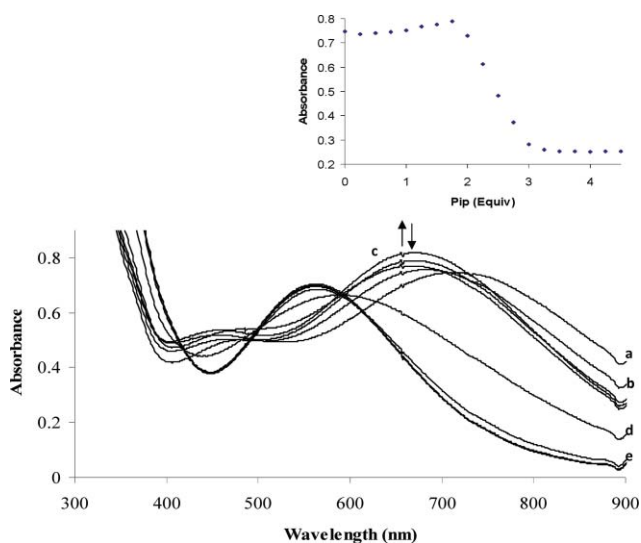
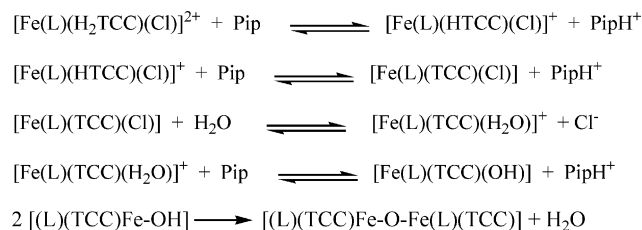


**Fig. 3** Spectrophotometric titration of a solution of [Fe(L<sub>2</sub>)Cl<sub>3</sub>] **2** (4 × 10<sup>-4</sup> M) and H<sub>2</sub>TCC (4 × 10<sup>-4</sup> M) against piperidine (0.3 M) (a: 0.0, b: 0.5, c: 2, d: 2.25, e: 3 equivalents). Inset: plot of absorbance vs. base equivalents at 745 nm.

appears around 560 nm with the spectrum obtained being very similar to that obtained for the dinuclear complex **7** (*cf.* above). This suggests the spontaneous formation of the dinuclear complex from the mononuclear species and water impurity in solution upon adding the third equivalent of base (Scheme 3). The catecholate dianion chelates with iron(III) symmetrically as seen from the observation of only one iron(III)-to-catecholate LMCT band.



**Scheme 3** Proposed pathway for the formation of μ-oxo dimeric complex.

### Electrochemical behavior

The electrochemical features of the iron(III) complexes and their DBC<sup>2-</sup> adducts generated *in situ* in DMF solution were investigated by employing cyclic (CV) and differential pulse voltammetry (DPV) on a stationary platinum sphere electrode. The iron(III) complexes **1–6** exhibit a coupled pair of redox waves at negative potentials, which are assigned<sup>14,21,30,31</sup> to Fe<sup>III</sup>/Fe<sup>II</sup> couple (Fig. 4; Table 4). The Fe<sup>III</sup>/Fe<sup>II</sup> redox potentials (−0.306 to −0.372 V) of

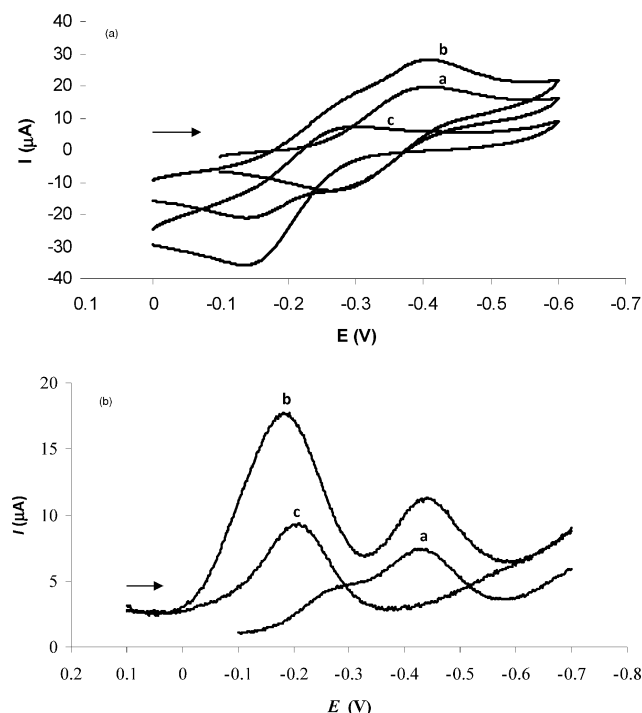


**Fig. 4** (top) Cyclic voltammograms of 1 mM [Fe(L<sub>2</sub>)Cl<sub>3</sub>] **2** (a), with 1 mM H<sub>2</sub>DBC added (b) and 1 mM H<sub>2</sub>DBC and 2 mM triethylamine added (c) in DMF solution at 25 °C. Supporting electrolyte: 0.1 M TBAP. Scan rate: 0.050 V s<sup>-1</sup>. (bottom) Differential pulse voltammograms of 1 mM [Fe(L<sub>4</sub>)Cl<sub>3</sub>] **4** without (a), and with 1 mM of H<sub>2</sub>DBC added (b) and 1 mM of H<sub>2</sub>DBC and 2 mM triethylamine added (c) in DMF solution at 25 °C. Scan rate 0.005 V s<sup>-1</sup>.

**Table 4** Electrochemical data<sup>a</sup> for [Fe(L)Cl<sub>3</sub>] and [Fe(L)(DBC)Cl]<sup>b</sup> in dimethylformamide at 25.0 ± 0.2 °C at a scan rate of 0.05 V s<sup>-1</sup> (CV) and 0.005 V s<sup>-1</sup> (DPV)

Complexes	$E_{1/2}/V$		Complexes	$E_{1/2}/V$		Redox process
	CV	DPV		CV	DPV	
[Fe(L1)Cl <sub>3</sub> ]	-0.343	-0.306	[Fe(L4)Cl <sub>3</sub> ]	-0.422	-0.432	Fe <sup>III</sup> → Fe <sup>II</sup>
+ H <sub>2</sub> DBC	-0.239	-0.256	+ H <sub>2</sub> DBC	-	-0.290 <sup>c</sup>	DBSQ → H <sub>2</sub> DBC
[Fe(L1)(DBC)Cl]	-0.318	-0.306	[Fe(L4)(DBC)Cl]	-0.203	-0.182	Fe <sup>III</sup> → Fe <sup>II</sup>
	-0.318	-0.306		-0.433	-0.438	DBSQ → DBC <sup>2-</sup>
	-0.228	-0.214		-	-0.208	Fe <sup>III</sup> → Fe <sup>II</sup>
[Fe(L2)Cl <sub>3</sub> ]	-0.336	-0.318	[Fe(L5)Cl <sub>3</sub> ]	-	-0.444	Fe <sup>III</sup> → Fe <sup>II</sup>
+ H <sub>2</sub> DBC	-0.219	-0.218	+ H <sub>2</sub> DBC	-	-	DBSQ → H <sub>2</sub> DBC
[Fe(L2)(DBC)Cl]	-0.339	-0.338	[Fe(L5)(DBC)Cl]	-0.517	-0.492	Fe <sup>III</sup> → Fe <sup>II</sup>
	-0.219	-0.188		-	-0.186	DBSQ → DBC <sup>2-</sup>
[Fe(L3)Cl <sub>3</sub> ]	-	-	[Fe(L6)Cl <sub>3</sub> ]	-	-	Fe <sup>III</sup> → Fe <sup>II</sup>
+ H <sub>2</sub> DBC	-	-0.372	+ H <sub>2</sub> DBC	-0.361	-0.398	DBSQ → H <sub>2</sub> DBC
[Fe(L3)(DBC)Cl]	-	-	[Fe(L6)(DBC)Cl]	-	-0.265 <sup>c</sup>	Fe <sup>III</sup> → Fe <sup>II</sup>
	-	-		-0.217	-0.174	DBSQ → H <sub>2</sub> DBC
	-	-		-0.503	-0.482	Fe <sup>III</sup> → Fe <sup>II</sup>
	-	-		-	-0.186	DBSQ → DBC <sup>2-</sup>
	-	-		-	-	Fe <sup>III</sup> → Fe <sup>II</sup>

<sup>a</sup> Potential measured vs. Ag(s)/AgNO<sub>3</sub> (0.01 M, 0.10 M TBAP); add 0.544 V to convert to NHE. <sup>b</sup> Generated by adding one equivalent of H<sub>2</sub>DBC and two equivalents of triethylamine to complex [Fe(L)Cl<sub>3</sub>]. <sup>c</sup> Additional cathodic wave corresponding to [Fe(L)(Sol)Cl<sub>3</sub>]<sup>+</sup> species.<sup>14d</sup>

the complexes of the imidazole ligands follow the trend **1** > **2** > **3** reflecting a decrease in Lewis acidity of iron(III) center along this series. With the replacement of the pyridyl moiety in **1** by the electron-releasing groups as in **2** and **3**, the Lewis acidity of iron(III) center decreases. The Fe<sup>III</sup>/Fe<sup>II</sup> redox potentials of the pyrazole-based complexes **4–6** (–0.398 to –0.444 V) are more negative than those for the pyridyl-based complexes **1–3** clearly suggesting that the tripodal ligands are more strongly coordinated than the linear ligands. The Fe<sup>III</sup>/Fe<sup>II</sup> redox potentials of the tripodal ligand complexes follow the trend **6** > **4** > **5**, which represents a decrease in Lewis acidity of the iron(III) center along this series. On introducing the *iso*-propyl group on the 3-position of pyrazole rings in **4** to give **6**, the sterically hindering *iso*-propyl group weakens the coordination of N2 nitrogen of pyrazolyl ring leading to confer an enhanced Lewis acidity of the iron(III) center. The electron-releasing methyl groups on the pyrazole ring in **5** increases the electron density on pyrazole N2 nitrogen and hence decreases the Lewis acidity of the iron(III) center.

On adding one equivalent of H<sub>2</sub>DBC to **1–6** in DMF solution a new wave appears in the CV and DPV responses (Fig. 4), which corresponds to the DBSQ/DBC<sup>2-</sup> couple<sup>20,21,30,31</sup> of [Fe(L)(DBC)Cl] species generated. On adding two equivalents of Et<sub>3</sub>N to deprotonate the catechol the reduction current of this couple increases and the Fe<sup>III</sup>/Fe<sup>II</sup> redox wave tends to vanish completely, which is expected<sup>10,14,21,30,31</sup> to be shifted to a more negative potential due to chelation of DBC<sup>2-</sup>. The redox potential of DBSQ/DBC<sup>2-</sup> couple of [Fe(L)(DBC)Cl] species is observed in the narrow range of –0.188 to –0.214 V (Table 4), which is less negative than that of free DBSQ/DBC<sup>2-</sup> couple ( $E_{pc}$ , –1.34 V vs. SCE).<sup>41</sup> Thus the extent of stabilization of the semiquinone radical of DBC<sup>2-</sup> towards oxidation is found to be the same for both the linear and tripodal tridentate ligand complexes in spite of the lower Lewis acidity of the iron(III) center observed for the latter complexes (*cf.* above). It is possible that upon DBC<sup>2-</sup> coordination one of the tripodal arms in **4–6** dissociate leading to an increase in Lewis acidity of the iron(III) center and hence the same extent of

stabilization of the semiquinone radical towards oxidation for both the imidazole- and pyrazole-based complexes. In this regard it is interesting to note that the  $E_{1/2}$  values of DBSQ/DBC<sup>2-</sup> couple for the adducts of terminal amine substituted 3 N ligand complexes<sup>31</sup> are more negative (–0.209 to –0.223 V) than those (–0.045 to +0.025 V) for the central amine substituted BPA complexes.<sup>30</sup> This reveals that the DBSQ/DBC<sup>2-</sup> couple of the catecholate adducts are sensitive to the iron(III) environment as modified by the ligand substituents. It is obvious that the electronic environment around iron(III) in both the imidazole- and pyrazole-based complexes is the same, which is possibly achieved by dissociation of one of the three arms of the tripodal ligand complexes from the coordination sphere upon DBC<sup>2-</sup> coordination. This is consistent with the small differences in LMCT spectral band positions between the two types of complexes.

### Dioxygenase activity

The catecholate adducts [Fe(L)(DBC)Cl] and [Fe(L)(DBC)(Sol)]<sup>+</sup> were generated *in situ* by treating respectively the complexes [Fe(L)Cl<sub>3</sub>] and [Fe(L)(Sol)<sub>3</sub>]<sup>3+</sup> (obtained<sup>30,31</sup> *in situ* by treating [Fe(L)Cl<sub>3</sub>] with three equivalents of AgClO<sub>4</sub>·H<sub>2</sub>O) with equimolar quantities of H<sub>2</sub>DBC and two equivalents of Et<sub>3</sub>N in DMF solvent and then exposed to molecular oxygen. The disappearance of the low energy catecholate-to-iron(III) LMCT band (Fig. 5) on oxygenation of the catecholate adducts exhibits pseudo-first order kinetics as judged from the linearity of the [1 + log(absorbance)] vs. time plot (Fig. 6) and the values of  $k_{obs}$  were obtained from the slopes of these plots. The second order rate constants were calculated<sup>17,18</sup> (Table 5) by using the equation,

$$k_{O_2} = k_{obs}/[O_2]$$

The products of the cleavage of H<sub>2</sub>DBC in DMF solvent (Table 5) were identified (**a–e**, Fig. 7) by GC-MS and <sup>1</sup>H NMR techniques and quantified by GC analysis. The complexes **1–3** with imidazole nitrogen donors afford major amounts

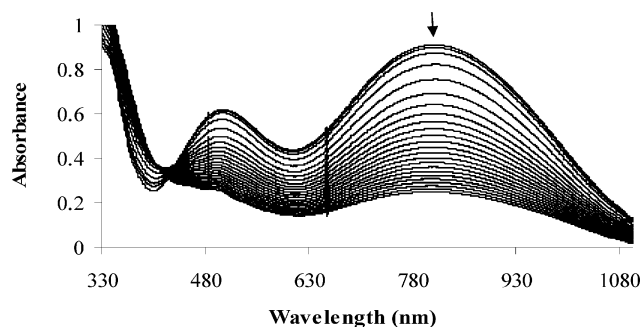


**Fig. 5** Progress of the reaction of adduct  $[\text{Fe}(\text{L}2)(\text{DBC})(\text{Sol})]^+$  with  $\text{O}_2$  in DMF solution. The disappearance of the  $\text{DBC}^{2-}$ -to-iron(III) charge-transfer band is monitored.

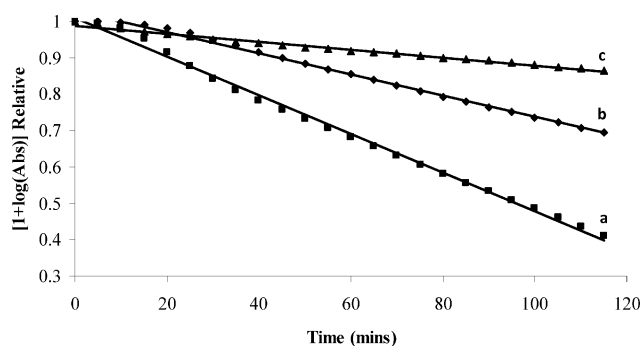


**Fig. 6** Plots of  $[1 + \log(\text{absorbance})]$  vs. time for the reaction of  $\text{Fe}(\text{L})(\text{DBC})(\text{Sol})^+$  with  $\text{O}_2$  at  $25^\circ\text{C}$  in DMF solution. Concentration of complexes,  $4 \times 10^{-4}$  M (a):  $[\text{Fe}(\text{L}2)(\text{DBC})(\text{Sol})]^+$ , (b):  $[\text{Fe}(\text{L}1)(\text{DBC})(\text{Sol})]^+$ , (c):  $[\text{Fe}(\text{L}3)(\text{DBC})(\text{Sol})]^+$ .

of the intradiol cleavage product (I) 3,5-di-*tert*-butyl-5-(*N,N*-dimethylamidomethyl)-2-furanone (**a**) and smaller amounts of the extradiol cleavage products (E) 3,5-di-*tert*-butyl-2-pyrone (**c**) and 4,6-di-*tert*-butyl-2-pyrone (**d**) in DMF solvent with the extradiol to intradiol product selectivity (E:I) varying from 0.14:1 to 0.45:1. Interestingly, when the coordinated chloride ion in  $[\text{Fe}(\text{L})(\text{DBC})\text{Cl}]$  is removed to generate  $[\text{Fe}(\text{L})(\text{DBC})(\text{Sol})]^+$  species in DMF solvent, the product selectivity (E:I) increases to 0.6:1–1.8:1, with the adduct  $[\text{Fe}(\text{L}2)(\text{DBC})(\text{Sol})]^+$  giving

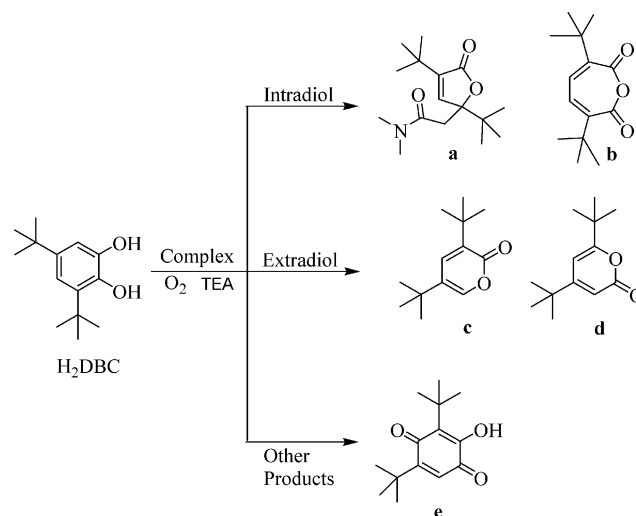


**Fig. 7** Products of catechol cleavage of 3,5-di-*tert*-butylcatechol ( $\text{H}_2\text{DBC}$ ) mediated by the iron(III) complexes: 3,5-di-*tert*-butyl-5-(*N,N*-dimethylamidomethyl)-2-furanone (**a**), 3,5-di-*tert*-butyl-1-oxacyclohepta-3,5-diene-2,7-dione (**b**), 3,5-di-*tert*-butyl-2-pyrone (**c**), 4,6-di-*tert*-butyl-2-pyrone (**d**), and 3,5-di-*tert*-butyl-2-hydroxy-1,4-benzoquinone (**e**).

38% yield of extradiol products. The second order reaction rate constants ( $k_{\text{O}_2}$ ,  $0.79\text{--}4.02 \times 10^{-2} \text{ M}^{-1} \text{ s}^{-1}$ , Table 5) for the adducts  $[\text{Fe}(\text{L})(\text{DBC})(\text{Sol})]^+$  derived from **1–3** in DMF are higher than those ( $k_{\text{O}_2}$ ,  $0.59\text{--}2.40 \times 10^{-2} \text{ M}^{-1} \text{ s}^{-1}$ ) for the respective adducts  $[\text{Fe}(\text{L})(\text{DBC})\text{Cl}]$  in the same solvent. In contrast to the iron(III) complexes **1–3** of imidazole-based ligands, those of the tripodal pyrazole-based ligands (**4–6**) effect the oxidation of  $\text{H}_2\text{DBC}$  on exposure to  $\text{O}_2$  to afford mainly the benzoquinone product (**e**); also, small amounts of extradiol cleavage products (**c** and **d**) and very small amounts of intradiol cleavage products (**a** and **b**) are also obtained. So, the second order reaction rate constants observed ( $k_{\text{O}_2}$ ,  $1.85\text{--}2.39 \times 10^{-2} \text{ M}^{-1} \text{ s}^{-1}$ , Table 5) for the  $[\text{Fe}(\text{L})(\text{DBC})\text{Cl}]$  adducts of **4–6** with pyrazolyl ligands in DMF (Table 3) correspond mainly to two-electron oxidation of catechol.

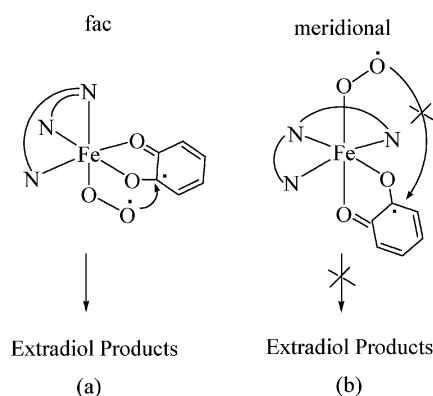
The dioxygenase activity of **1–3** can be illustrated by invoking the substrate activation mechanism proposed<sup>8</sup> for intradiol-cleaving enzymes. Thus,  $\text{O}_2$  attacks the iron(III)-bound catecholate

**Table 5** Kinetic data<sup>a</sup> for the catalytic reaction and quantification of cleavage products (% yield)

Complex	Intradiol (%)	Extradiol (%)	E : I ratio	Quinone (%)	Reaction rate ( $\times 10^{-2} \text{ M}^{-1} \text{ s}^{-1}$ )
$[\text{Fe}(\text{L}1)\text{Cl}_3]$	43.1 ( <b>a</b> )	12.0 ( <b>c</b> )	0.27 : 1	—	$0.59 \pm 0.03$
$[\text{Fe}(\text{L}1)(\text{Sol})]^{3+}$	26.0 ( <b>a</b> )	9.7 ( <b>c</b> ) 5.5 ( <b>d</b> )	0.58 : 1	—	$2.25 \pm 0.01$
$[\text{Fe}(\text{L}2)\text{Cl}_3]$	24.7 ( <b>a</b> )	11.1 ( <b>c</b> )	0.45 : 1	—	$0.21 \pm 0.01$
$[\text{Fe}(\text{L}2)(\text{Sol})]^{3+}$	21.3 ( <b>a</b> )	27.9 ( <b>c</b> ) 11.0 ( <b>f</b> )	1.83 : 1	—	$4.02 \pm 0.04$
$[\text{Fe}(\text{L}3)\text{Cl}_3]$	40.7 ( <b>a</b> )	6.0 ( <b>c</b> )	0.14 : 1	—	$2.40 \pm 0.02$
$[\text{Fe}(\text{L}3)(\text{Sol})]^{3+}$	18.2 ( <b>a</b> )	20.4 ( <b>c</b> )	1.09 : 1	—	$0.79 \pm 0.001$
$[\text{Fe}(\text{L}4)\text{Cl}_3]$ <b>4</b>	<b>a</b> (2.0) <b>b</b> (3.0)	—	—	<b>e</b> (40.0)	$1.85 \pm 0.02$
$[\text{Fe}(\text{L}5)\text{Cl}_3]$ <b>5</b>	<b>b</b> (1.8)	<b>c</b> (11.8) <b>d</b> (1.5)	—	<b>e</b> (22.3)	$1.90 \pm 0.01$
$[\text{Fe}(\text{L}6)\text{Cl}_3]$ <b>6</b>	<b>b</b> (2.9)	<b>c</b> (2.0) <b>d</b> (4.0)	—	<b>e</b> (16.3)	$2.39 \pm 0.01$

<sup>a</sup>  $k_{\text{O}_2} = k_{\text{obs}}/[\text{O}_2]$ . The solubility of  $\text{O}_2$  in DMF at  $25^\circ\text{C}$  is 4.86 mM. The kinetic data were obtained by monitoring the disappearance of the lower energy LMCT band.

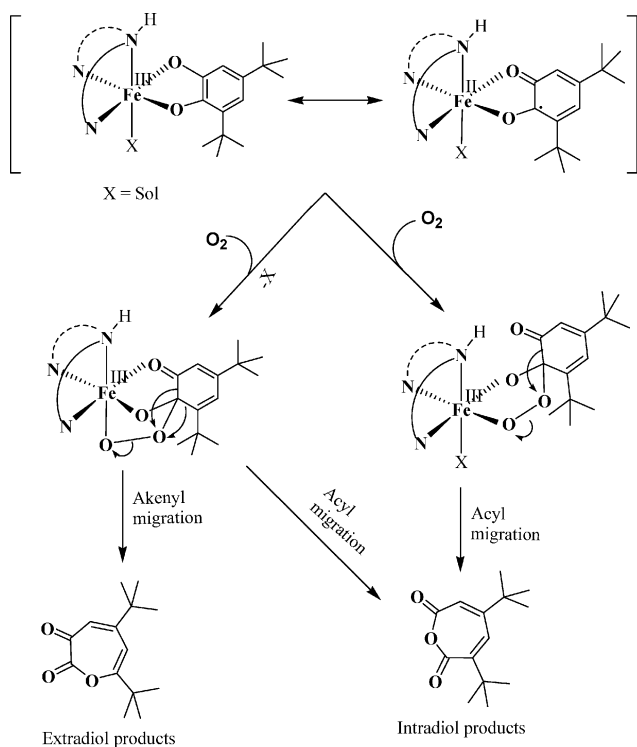
in  $[\text{Fe}(\text{L})(\text{DBC})\text{Cl}]$  to form the substrate–alkylperoxo– $\text{Fe}^{3+}$  intermediate  $[(\text{L})(\text{DBSQ})\text{Fe}(\text{III})\text{O}_2]^-$ , which gives intradiol cleavage products upon acyl migration and extradiol cleavage products upon alkenyl migration (Scheme 4). The formation of extradiol cleavage products can also be explained by invoking the extradiol cleavage mechanism,<sup>39,40</sup> which involves the attack of molecular oxygen on iron(III). This mechanism has been used to illustrate the nearly quantitative yield of the oxidative extradiol cleavage products<sup>28</sup> observed for the reaction of molecular oxygen with  $[\text{Fe}(\text{Me}_3\text{tacn})(\text{DBC})\text{Cl}]$ , which contains facially coordinated ligands. Similarly, for the adduct  $[\text{Fe}(\text{BBA})(\text{DBC})]\text{ClO}_4$ , where BBA is bis(benzimidazol-2-ylmethyl)amine, a large amount (60%) of the extradiol cleavage products **c** and **d** has been observed<sup>26</sup> upon oxygenation. Also, the six-coordinate octahedral complex  $[\text{Fe}(\text{Tp}^{\text{Pr}_2})(\text{DBC})(\text{CH}_3\text{CN})]$  gives the extradiol cleavage products in 70% yield.<sup>27</sup> The facial coordination of ligands in all these adducts allow both  $\text{O}_2$  and substrate to occupy the opposite face to form the intermediate<sup>22</sup>  $[(\text{L})(\text{DBSQ})\text{Fe}(\text{III})-\text{O}_2]^-$ , which is the same as that obtained in the above intradiol cleavage mechanism (Scheme 5(a)). Very recently, the key peroxide intermediate, along with the  $\text{O}_2$  adduct precursor and the product complex successor to the intermediate, has been found to be present in the X-ray crystal structures of different subunits of the homoprotocatechuate 2,3-dioxygenase enzyme reacted with 4-nitrocatechol as substrate.<sup>40</sup> By invoking the same alkylperoxo intermediate with iron(III) oxidation state we have previously explained the formation of varying amounts of intradiol and extradiol cleavage products for the iron(III) complexes of the pyridyl analogues of **L1–L3** ligands,<sup>21</sup> differently substituted bis(pyrid-2-ylmethyl)amine (BPA) ligands<sup>31</sup> and sterically constrained 4N<sup>34</sup> ligands has been also explained. On the other hand, meridional coordination of a 3N ligand



**Scheme 5** Facial (a) and meridional (b) coordination of 3 N ligands leading to different cleavage products.

like TPY in  $[\text{Fe}(\text{TPY})(\text{DBC})]^+$  yields major amounts of quinone product (78%) in addition to intradiol cleavage product (20%) (Scheme 5(b)).<sup>28</sup> The  $\text{O}_2$  molecule bound to iron(III) is constrained to be in the same plane as that of the catecholate substrate, which it cannot attack, but transfers two electrons through the iron(III) center to the substrate leading to the oxidation to catechol to give the quinone product. So, it is expected that upon oxygenation the  $\text{DBC}^{2-}$  adducts of **1–3** also would yield extradiol products since the ligands are facially coordinated and a coordination position is vacant for dioxygen binding. The increase in product selectivity (E:I) upon removal of the coordinated chloride ion in these adducts  $[\text{Fe}(\text{L})(\text{DBC})\text{Cl}]$  to generate  $[\text{Fe}(\text{L})(\text{DBC})(\text{Sol})]^+$  species in DMF solvent clearly indicates that the presence of a vacant or solvent-coordinated site on iron(III) center of the catecholate adducts is essential for dioxygen attack to achieve extradiol cleavage products and that a coordinated chloride ion in the adduct  $[\text{Fe}(\text{L})(\text{DBC})\text{Cl}]$  is difficult to be replaced by dioxygen to afford extradiol cleavage products.<sup>30,31</sup> Also, the observation of a higher E:I value for  $[\text{Fe}(\text{L2})(\text{DBC})\text{Cl}]$  reveals that the sterically hindering terminal  $-\text{NMe}_2$  group of the ligand appears to be oriented away from the  $\text{sp}^3$  hybridized carbon atom of the catecholate substrate in the above alkylperoxo intermediate and facilitates alkenyl migration to give enhanced regioselective extradiol cleavage products.<sup>30</sup> Also, upon replacement of one of the pyridyl moieties in the 1:1 iron(III) complex<sup>30</sup> of *N'*-(pyrid-2-ylmethyl)-*N,N*-dimethylethylenediamine by *N*-Me-imidazolyl moiety to get  $[\text{Fe}(\text{L2})(\text{DBC})\text{Cl}]$  a dramatic decrease in product selectivity (E:I) from 18.5:1.0 to 1.83:1.0 is observed. Obviously, the sterically less hindering *N*-Me-imidazolyl moiety favours the attack of molecular oxygen and also facilitates acyl rather than alkenyl migration to give intradiol cleavage products.

The second order reaction rate constants ( $k_{\text{O}_2}$ ,  $0.79\text{--}4.02 \times 10^{-2} \text{ M}^{-1} \text{ s}^{-1}$ , Table 5) for the adducts  $[\text{Fe}(\text{L})(\text{DBC})(\text{Sol})]^+$  derived from **1–3** in DMF are higher than those ( $k_{\text{O}_2}$ ,  $0.59\text{--}2.40 \times 10^{-2} \text{ M}^{-1} \text{ s}^{-1}$ ) for the respective adducts  $[\text{Fe}(\text{L})(\text{DBC})\text{Cl}]$  in the same solvent. This is expected of the higher Lewis acidity<sup>10</sup> of the iron(III) center in  $[\text{Fe}(\text{L})(\text{DBC})(\text{Sol})]^+$  adducts, which favours both catecholate and dioxygen binding. As the sterically demanding *N*-Ph substituent on the primary ligand in  $[\text{Fe}(\text{L3})(\text{DBC})\text{Cl}]$  would hinder the fast approach of dioxygen a decreased rate is expected for the complex.<sup>16,27</sup> However, interestingly, this adduct shows the highest rate of oxygenation among the present complexes obviously because the sterically demanding *N*-Ph substituent

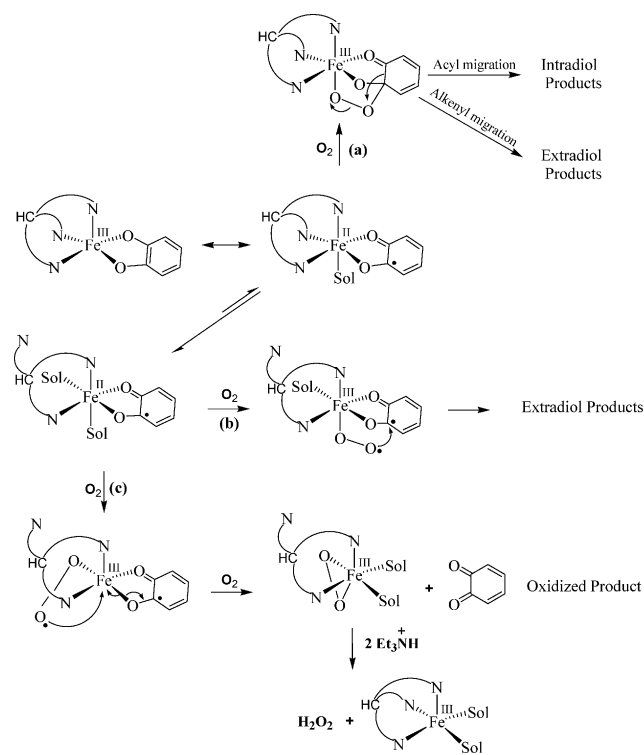


**Scheme 4** Proposed mechanism for oxidative cleavage of  $\text{H}_2\text{DBC}$  by dioxygen catalysed by **1–3**.

strengthens the iron(III)–catecholate interaction in the alkylperoxo intermediate  $[(L3)(DBSQ)Fe(III)O_2]^-$  by increasing the Lewis acidity of the iron(III) center and thus enhances the rate of formation of both the intra- and extradiol cleavage products (*cf.* above).<sup>31</sup> Interestingly, the rate of cleavage of  $[Fe(L2)(DBC)(Sol)]^+$  species is higher than the other two solvated adducts suggesting that the sterically less hindering *N*-Me-imidazolyl moiety, supported by the higher Lewis acidity of the iron(III) center, favours the attack of molecular oxygen. Thus, the trend in the observed yields of dioxygenase reaction of complexes could be illustrated solely on the basis of the steric hindrance to substrate and  $O_2$  binding while the trend in the observed values of  $k_{O_2}$  on the basis of Lewis acidity of the iron(III) center, better by a delicate balance between these two factors.

As illustrated above for 1–3, the  $DBC^{2-}$  adducts of 4–6 are also expected to yield extradiol cleavage products upon oxygenation since they contain the tripodal ligands facially coordinated and also a coordination position vacant for dioxygen binding. However, interestingly, all of them yield mainly the oxidized product benzoquinone. It is clear that they are not prone to form the intermediate  $[(L)(DBSQ)Fe(III)O_2]^-$  responsible for catechol cleavage. Funabiki *et al.* have found<sup>13</sup> that the complex  $[Fe(BPY)(DBC)(H_2O)_2]$ , where BPY is 2,2'-bipyridine, yields mainly the oxidized product benzoquinone upon oxygenation. They have also reported<sup>13</sup> the formation of benzoquinone when  $FeCl_3/BPY/Py$  was used for dioxygenation of catechol in THF solution. Thus, the formation of the oxidized products for 4–6 can be explained by assuming equatorial attack of dioxygen on the  $DBC^{2-}$  adducts of the complexes (Scheme 6(c)) in which one of the arms of the tripodal ligand (*trans* to one of the strong Fe–O(catecholate) bonds) is displaced from the octahedral coordination sphere due to the sterically constrained 6,6,6-chelate ring system. The equatorially bound dioxygen is unable to attack the semiquinone radical located in the same plane and hence the oxidation product benzoquinone is formed in larger amounts as for the BPY and TERPY complexes (Scheme 5(b)). The extradiol cleavage products are obtained when dioxygen attacks the axial position of the adduct with (Scheme 6(b)) or without (Scheme 6(a)) dissociation of one of the arms of the tripodal ligand (Scheme 6(c)), while the intradiol cleavage products are formed (Scheme 6(a)) by the concerted<sup>8</sup> dioxygen attack on iron(III) and the carbon atom of the bound catecholate.

The yield of quinone product for the  $[Fe(L)(DBC)Cl]$  adducts of 4–6 with pyrazolyl ligands in DMF decreases along the series 4 > 5 > 6 (Table 3) while their second order reaction rate constants vary in the order 6 > 5 ~ 4. As substrate binding is the first step in the mechanism (Scheme 6(c)), the highest Lewis acidity of 6 (*cf.* above) would encourage its strongest binding with both anionic  $DBC^{2-}$  and dioxygen leading to the highest yield of the benzoquinone product. However, only a low yield of quinone is observed revealing that the bulky *iso*-propyl substituent on the pyrazole ring in 6 sterically hinders the binding of  $DBC^{2-}$ , which is verified by building molecular models. Indeed, a decreased dioxygenase activity has been found upon introducing bulky alkyl groups near the donor atoms in the heterocyclic ring systems<sup>26</sup> in  $[Fe(Tp^{iPr,Bu})(DBC)]^+$  and  $[Fe(6-MeTPA)(DBC)]^+$ . Similarly, the catecholate adduct of 6 with a sterically hindering *iso*-propyl substituent (*cf.* above) would be expected to show a decreased rate of quinone formation but it exhibits the highest rate of



Scheme 6

reaction. Therefore, it appears that the bulky *iso*-propyl groups on the pyrazolyl ring in 6 do not hinder the approach of  $DBC^{2-}$  and dioxygen and it is the highest Lewis acidity of 6 which strengthens the iron(III)–catecholate interaction in the alkylperoxo intermediate  $[(L6)(DBSQ)Fe(III)O_2]^-$  leading to facile dioxygen attack and hence the highest rate of dioxygenation is observed.<sup>30,31</sup> Also, the dissociation of one of the sterically hindering pyrazolyl arms from the coordination sphere (*cf.* above) would lead to an increase in Lewis acidity of the iron(III) center. Thus it is remarkable that the iron(III) complexes with facially coordinated tris(pyrazolyl)methane ligand yields only the quinone product obviously due to bidentate coordination of the tripodal ligand. Also, for complexes of both the imidazole- and pyrazole-based 3N ligands the steric constraint around iron(III) determines the yield of dioxygenation products while the Lewis acidity of the iron(III) center determines the observed rates of dioxygenation.

## Experimental

### Materials

The chemicals iron(III) chloride (anhydrous) ( $FeCl_3$ ), 1-methyl-2-imidazolecarboxaldehyde, aminomethylpyridine, *N*-phenylethylenediamine, *N,N*-dimethylethylenediamine, sodium borohydride, 2-methyl-3-butanone, 3,5-di-*tert*-butylcatechol ( $H_2DBC$ ), 3-methylcatechol (3-MeH<sub>2</sub>CAT), (Aldrich Chemicals), 3,4,5,6-tetrachlorocatechol ( $H_2TCC$ ) (Lancaster), catechol ( $H_2CAT$ ) (Loba India), acetylacetone, hydrazine hydrochloride, chloroform, ethyl formate, sodium methoxide, triethylamine (Merck, India), and pyrazole (Fluka), were used as received. Methanol, acetonitrile, dichloromethane, dimethylformamide and diethylether were purchased from Merck, India. The supporting

electrolyte tetra-*N*-butylammonium perchlorate (TBAP) was prepared by using a procedure reported<sup>41</sup> already.

### Preparation of the ligands L1–L6

The ligands L1–L3 were synthesized using the method reported in the literature.<sup>30</sup> Pyrazole, 3,5-dimethylpyrazole and 3-*iso*-propylpyrazole required for the syntheses of ligands L4–L6 were either purchased or prepared by the already reported procedures.<sup>35,36</sup>

#### 1-Methyl-1*H*-imidazol-2-ylmethyl-(pyrid-2-ylmethyl)amine

**(L1).** 1-Methyl-2-imidazolecarboxaldehyde (1.10 g, 10 mmol) in methanol (20 mL) was added dropwise to aminomethylpyridine (1.08 g, 10 mmol) in methanol (20 mL). The mixture was stirred overnight and then NaBH<sub>4</sub> (0.57 g, 15 mmol) was added and the solution was stirred for another day and then rotaevaporated to dryness. The resulting solid was dissolved in water and then extracted with dichloromethane. The organic layer was dried with anhydrous sodium sulfate and then rotaevaporated to obtain the ligand as an oil. Yield: 1.32 g (65.3%); C<sub>11</sub>H<sub>14</sub>N<sub>4</sub> (202.26). <sup>1</sup>H NMR (200 MHz, CDCl<sub>3</sub>): δ 8.44–7.26 (m, 4H), 6.72 (s, 1H), 6.62 (s, 1H), 4.14 (s, 2H), 3.81 (s, 2H), 3.63 (s, 3H).

***N,N*-Dimethyl-*N'*-(1-methyl-1*H*-imidazol-2-ylmethyl)ethane-1,2-diamine (L2).** The ligand L2 was prepared by the same procedure employed for L1, except that the amine used here was *N,N*-dimethylethylenediamine (0.88 g, 10 mmol). Yield: 1.23 g (67.5%); C<sub>9</sub>H<sub>18</sub>N<sub>4</sub> (182.27). <sup>1</sup>H NMR (200 MHz, CDCl<sub>3</sub>): δ 6.72 (s, 1H), 6.62 (s, 1H), 3.81 (s, 2H), 3.63 (s, 3H), 2.65–2.48 (m, 4H), 2.27 (s, 6H).

***N*-(1-Methyl-1*H*-imidazol-2-ylmethyl)-*N'*-phenylethane-1,2-diamine (L3).** The ligand L3 was prepared by the same procedure employed for L1, except that the amine used here was *N*-phenylethylenediamine (1.36 g, 10 mmol). Yield: 0.88 g (73%); C<sub>13</sub>H<sub>18</sub>N<sub>4</sub> (230.31). <sup>1</sup>H NMR (200 MHz, CDCl<sub>3</sub>): δ 6.43–7.04 (m, 5H), 6.72 (s, 1H), 6.62 (s, 1H), 4.14 (s, 1H), 3.81 (s, 2H), 3.63 (s, 3H), 2.72–3.2 (m, 4H).

### Preparation of iron(III) complexes

**[Fe(L1)Cl<sub>3</sub>] (1).** The complex [Fe(L1)Cl<sub>3</sub>] **1** was prepared by adding anhydrous FeCl<sub>3</sub> (0.16 g, 1 mmol) in methanol (10 mL) to a solution of the ligand L1 (0.20 g, 1 mmol) in methanol (10 mL) with stirring. The yellow colored complex was filtered off, washed with cold methanol and diethylether and then dried under vacuum. Yield: 0.24 g (75%). Anal. Calcd for C<sub>11</sub>H<sub>14</sub>Cl<sub>3</sub>FeN<sub>4</sub> (364.46): C, 36.25; H, 3.87; N, 15.37. Found: C, 36.23; H, 3.90; N, 15.36. ESI-MS *m/z* = 329 [Fe(L1)Cl<sub>2</sub>]<sup>+</sup>.

**[Fe(L2)Cl<sub>3</sub>] (2).** This was isolated using a procedure analogous to that used to prepare **1** using L2 (0.18 g, 1 mmol) instead of L1. The pure product was isolated as an orange colored precipitate. Yield: 0.17 g (50%). Anal. Calcd for C<sub>9</sub>H<sub>18</sub>Cl<sub>3</sub>FeN<sub>4</sub> (344.47): C, 31.38; H, 5.27; N, 16.26. Found: C, 31.35; H, 5.25; N, 16.31. ESI-MS *m/z* = 308 [Fe(L2)Cl<sub>2</sub>]<sup>+</sup>.

**[Fe(L3)Cl<sub>3</sub>] (3).** A procedure analogous to that used to prepare **1** was followed to isolate this complex as a dark brown precipitate and L3 (0.23 g, 1 mmol) instead of L1 was employed. The solution was stirred and filtered which resulted in the formation of **3**. Yield:

0.21 g (55%). Anal. Calcd for C<sub>13</sub>H<sub>18</sub>Cl<sub>3</sub>FeN<sub>4</sub> (392.51): C, 39.78; H, 4.62; N, 14.27. Found C, 39.81; H, 4.69; N, 14.17. ESI-MS *m/z* = 357 [Fe(L3)Cl<sub>2</sub>]<sup>+</sup>.

**[Fe(L4)Cl<sub>3</sub>] (4).** A procedure analogous to that used to prepare **1** was followed to prepare this complex from L4. The pale yellow colored microcrystalline product was filtered off, washed with small amounts of cold methanol and then dried. Yield: 0.28 g (75%). Anal. Calcd for C<sub>10</sub>H<sub>10</sub>N<sub>6</sub>FeCl<sub>3</sub> (376.43): C, 31.91; H, 2.68; N, 22.33. Found: C, 31.81; H, 2.73; N, 22.38. ESI-MS, *m/z* = 339 [Fe(L4)Cl<sub>2</sub>]<sup>+</sup>.

**[Fe(L5)Cl<sub>3</sub>] (5).** The complex was isolated as an orange colored powder using the procedure employed for isolating **4**. Yield: 0.28 g (62%). Anal. Calcd for C<sub>16</sub>H<sub>22</sub>N<sub>6</sub>FeCl<sub>3</sub> (460.59): C, 41.72; H, 4.81; N, 18.25. Found: C, 41.60; H, 4.95; N, 18.23. ESI-MS, *m/z* = 424 [Fe(L5)Cl<sub>2</sub>]<sup>+</sup>.

**[Fe(L6)Cl<sub>3</sub>] (6).** The complex was prepared as dark yellow colored powder using the procedure employed for **4**. Yield: 0.25 g (51%). Anal. Calcd for C<sub>19</sub>H<sub>28</sub>N<sub>6</sub>FeCl<sub>3</sub> (502.67): C, 45.40; H, 5.61; N, 16.72. Found: C, 45.45; H, 5.58; N, 16.70%. ESI-MS, *m/z* = 466 [Fe(L6)Cl<sub>2</sub>]<sup>+</sup>.

**[Fe(L2)(TCC)]<sub>2</sub>O·2(CH<sub>3</sub>)<sub>2</sub>CO·H<sub>2</sub>O (7).** To the ligand L2 (18.2 mg, 0.1 mmol) in acetonitrile, anhydrous FeCl<sub>3</sub> in acetonitrile (16.2 mg, 0.1 mmol) was added. To this solution was added 3,4,5,6-tetrachlorocatechol (24.79 mg, 0.1 mmol) and then an excess of triethylamine (5 μL, 0.4 mmol) dissolved in acetonitrile. The mixture was stirred for a few minutes and then filtered. The filtrate was layered with acetone. Dark purple crystals of the adduct were formed within a few days upon slow cooling and standing. Yield: 0.05 g (55%). Anal. Calcd for C<sub>36</sub>H<sub>50</sub>Cl<sub>8</sub>Fe<sub>2</sub>N<sub>8</sub>O<sub>8</sub> (1114): C, 38.67; H, 4.51; N, 10.02. Found: C, 38.61; H, 4.59; N, 10.05.

### Physical measurements

Electronic spectral measurements in dimethylformamide solutions of the complexes were made with a Varian Cary 300 spectrophotometer. Cyclic voltammetry (CV) and differential pulse voltammetry (DPV) were performed using a three-electrode cell configuration. A platinum sphere, a platinum plate, and Ag(s)/AgNO<sub>3</sub> were used as working, auxiliary, and reference electrodes, respectively. The supporting electrolyte used was NBu<sub>4</sub>ClO<sub>4</sub>. The platinum sphere electrode was sonicated for 2 min in dilute nitric acid, dilute hydrazine hydrate, and then in double-distilled water to remove the impurities. The temperature of the electrochemical cell was maintained at 25 ± 0.2 °C by a cryocirculator (HAAKE D8 G). Bubbling research grade nitrogen deoxygenated the solutions, and an atmosphere of nitrogen was maintained over the solution during measurements. The *E*<sub>1/2</sub> values were observed under identical conditions for various scan rates. The instruments utilized included an EG&G PAR 273 potentiostat/galvanostat and a Pentium IV computer along with EG&G M270 software to carry out the experiments and to acquire the data. The redox potential (*E*<sub>1/2</sub>) was calculated from the anodic (*E*<sub>pa</sub>) and cathodic peak (*E*<sub>pc</sub>) potentials of CV traces as (*E*<sub>pa</sub> + *E*<sub>pc</sub>)/2. The redox potentials were also estimated from the DPV peak potentials (*E*<sub>p</sub>) using the relation,

$$E_{1/2} = E_p + \Delta E/2$$

where  $E_{1/2}$  is the equivalent of the average of  $E_{pc}$  and  $E_{pa}$  in CV experiments and  $\Delta E$  is the pulse amplitude. GC analyses were performed by HP (Hewlett Packard) 6890 GC series Gas Chromatograph equipped with a FID detector and a HP-5 capillary column (30 m  $\times$  0.32 mm  $\times$  2.5  $\mu$ m). GC-MS analysis was performed on a Perkin Elmer Clarus 500 GC-MS instrument using a PE-5 (HP-5 equivalent) capillary column.

### Crystallographic refinement and structure solution†

A crystal of a suitable size was selected from the mother liquor and immersed in paraffin oil, then mounted on the tip of a glass fiber and cemented using epoxy resin. Intensity data for the crystal were collected using Mo K $\alpha$  ( $\lambda = 0.71073$  Å) radiation on a Bruker SMART APEX diffractometer equipped with CCD area detector at 293 K. The crystallographic data are collected in Table 1. The SMART<sup>42</sup> program was used for collecting frames of data, indexing the reflections, and determination of lattice parameters; the SAINT<sup>42</sup> program was used for the integration of the intensity of reflections and scaling; the SADABS<sup>43</sup> program was used for absorption correction, and the SHELXTL<sup>44</sup> program for space group and structure determination, and least-squares refinements on  $F^2$ . The structure was solved by the heavy atom method. Other non-hydrogen atoms were located in successive difference Fourier syntheses. The final refinement was performed by full-matrix least-squares analysis. Hydrogen atoms attached to the ligand moiety were located from the difference Fourier map and refined isotropically.

### Dioxygenation studies

The catechol cleavage activity of all the complexes towards H<sub>2</sub>DBC was examined by exposing a solution of iron(III) complex–DBC<sup>2-</sup> adduct generated *in situ* in dimethylformamide (DMF) to molecular oxygen. Kinetic analyses of the catechol cleavage reactions were carried out by time dependent measurements of the disappearance of the lower energy DBC<sup>2-</sup>-to-iron(III) LMCT band in the presence and absence of chloride ions. Silver perchlorate monohydrate dissolved in DMF was used to remove chloride ions from the complex. Stock solutions (6.0  $\times$  10<sup>-3</sup> M) of the adducts [Fe(L)(DBC)(Cl)] and [Fe(L)(DBC)(Sol)]<sup>+</sup> were prepared by treating [Fe(L)Cl<sub>3</sub>] and [Fe(L)(Sol)<sub>3</sub>]<sup>3+</sup> complexes ([Fe(L)(Sol)<sub>3</sub>]<sup>3+</sup> was generated *in situ* by treatment with three equivalents of AgClO<sub>4</sub>·H<sub>2</sub>O in DMF and centrifuging the solution to remove AgCl) with an equivalent amount of H<sub>2</sub>DBC pretreated with two equivalents of Et<sub>3</sub>N. The oxygenation reaction was started by rapid delivery of a stock solution (0.2 mL) of the catecholate adducts (6.0  $\times$  10<sup>-3</sup> M) by a syringe to O<sub>2</sub>-saturated solvent (2.8 mL). The solubility of O<sub>2</sub> in DMF at 25 °C is 4.86 mM.<sup>5</sup> The product analysis was carried out by stirring the complex [Fe(L)(Sol)<sub>3</sub>]<sup>3+</sup> (0.1 mmol), H<sub>2</sub>DBC (0.1 mmol) and triethylamine (0.2 mmol) in DMF (20 mL) solvent under molecular oxygen over 4 h at room temperature. After the reaction was completed, the reaction mixture was concentrated under reduced pressure and extracted with diethylether (3  $\times$  5 mL). The remaining residue was acidified with HCl to pH 3 to decompose the metal complexes and extracted with diethylether (3  $\times$  5 mL). The combined extracts were dried over Na<sub>2</sub>SO<sub>4</sub>, and then concentrated. All the products were quantified using GC (FID) analysis with

the following temperature program: injector temperature 130 °C, initial temperature 60 °C, heating rate 10 °C min<sup>-1</sup> to 130 °C, then increasing at a rate of 2 °C min<sup>-1</sup> to 160 °C and then increasing at a rate of 5 °C min<sup>-1</sup> to 260 °C; FID temperature 280 °C. GC-MS analysis was performed under conditions identical to those used for GC analysis and the oxygenation products were identified by comparing the retention times already reported.<sup>30</sup> The oxidative cleavage products of H<sub>2</sub>DBC detected and identified (a–h) by GC-MS technique are depicted in Scheme 3.

### Conclusions

Mononuclear iron(III) complexes of both linear and tripodal tridentate 3N ligands containing imidazolyl and pyrazolyl moieties respectively, have been isolated and studied as functional models for catechol dioxygenases. One of the complexes with a facially coordinated imidazolyl ligand has been found to exhibit a tendency to dimerize in the presence of base upon binding to tetrachlorocatecholate. In DMF solution all the complexes of imidazole-based linear ligands elicit intradiol cleavage of di-*tert*-butylcatechol. Also, the extradiol-to-intradiol cleavage product selectivity increases upon replacing the coordinated chloride ions in these complexes by solvent, but it decreases upon incorporation of an imidazolyl nitrogen donor. In sharp contrast to these complexes, the pyrazole-containing tripodal ligand complexes yield mainly the oxidized product benzoquinone although the iron(III) electronic environments in the catecholate adducts of complexes of both the linear and tripodal tridentate ligands are almost the same, as revealed by the DBSQ/DBC<sup>2-</sup> redox potentials falling in the same narrow range. One of the pyrazolyl arms in the catecholate adducts is sterically constrained by the 6,6,6-chelate ring system and appears to dissociate from the coordination sphere upon binding to the catecholate substrate, which is followed by dioxygen attack at the equatorial plane leading to the formation of benzoquinone. Thus the present study reveals that a change in ligand topology of 1 : 1 iron(III) complexes of 3N ligands would lead to drastic changes in the dioxygenase reactivity pattern. Also, the yield of the quinone/cleavage product is found to decrease upon increasing the steric bulk of the ligands, while the rate of oxygenation increases upon increasing the Lewis acidity of the iron(III) center by modifying the ligand substituents.

### Acknowledgements

We sincerely thank the Council of Scientific and Industrial Research (CSIR), New Delhi for a Senior Research Fellowship to T. D. We also thank the Department of Science and Technology (DST), New Delhi for supporting this research [Scheme no. SR/S1/IC/45/2003 and SR/S5/BC-05/2006]. Professor M. Palaniandavar is the recipient of the Ramanna Fellowship from DST, New Delhi. We thank Professor K. Nataraajan, Bharathiar University, Coimbatore for CHN analysis and Dr Balachandran Unni Nair, Central Leather Research Institute, Chennai for ESI-MS spectra.

### References

- 1 S. Dagley, *Essays Biochem.*, 1975, **11**, 81.
- 2 T. D. H. Bugg and C. J. Winfield, *Nat. Prod. Rep.*, 1998, **15**, 513.

- 3 *Microbial Degradation of Organic Molecules*, ed. D. T. Gibson, Marcel Dekker, New York, 1984, p. 535.
- 4 W. Reineke and M. J. Knackmuss, *Annu. Rev. Microbiol.*, 1988, **42**, 263.
- 5 (a) L. Que, Jr and R. Y. N. Ho, *Chem. Rev.*, 1996, **96**, 2607; (b) A. L. Feig and S. J. Lippard, *Chem. Rev.*, 1994, **94**, 759.
- 6 (a) J. D. Lipscomb and A. M. Orville, in *Metal Ions in Biological Systems*, ed. H. Sigel and A. Sigel, Marcel Dekker, New York, 1992, vol. 28, pp 243–298; (b) L. Que, Jr, in *Iron Carriers and Iron Proteins*, ed. T. M. Loehr, VCH, New York, 1989, pp 467–524.
- 7 (a) D. H. Ohlendorf, J. D. Lipscomb and P. C. Weber, *Nature*, 1988, **336**, 403; (b) D. H. Ohlendorf, A. M. Orville and J. D. Lipscomb, *J. Mol. Biol.*, 1994, **244**, 586; (c) M. W. Vetting and D. H. Ohlendorf, *Structure*, 2000, **8**, 429.
- 8 (a) M. Y. M. Pau, M. I. Davis, A. M. Orville, J. D. Lipscomb and E. I. Solomon, *J. Am. Chem. Soc.*, 2007, **129**, 1944; (b) M. Y. M. Pau, J. D. Lipscomb and E. I. Solomon, *Proc. Natl. Acad. Sci. U. S. A.*, 2007, **104**, 18355.
- 9 (a) S. Han, L. D. Eltis, K. N. Timmis, S. W. Muchmore and J. T. Bolin, *Science*, 1995, **270**, 976; (b) N. Hayase, K. Taira and K. Furukawa, *J. Bacteriol.*, 1990, **172**, 1160; (c) P. A. Mabrouk, A. M. Orville, J. D. Lipscomb and E. I. Solomon, *J. Am. Chem. Soc.*, 1991, **113**, 4053; (d) K. Sugimoto, T. Senda, H. Aoshima, E. Masai, M. Fukuda and Y. Mitsui, *Structure*, 1999, **7**, 953.
- 10 (a) M. Costas, M. P. Mehn, M. P. Jensen and L. Que, Jr, *Chem. Rev.*, 2004, **104**, 939; (b) D. D. Cox and L. Que, Jr, *J. Am. Chem. Soc.*, 1988, **110**, 8085; (c) D. D. Cox, S. J. Benkovic, L. M. Bloom, F. C. Bradley, M. J. Nelson, L. Que, Jr and D. E. Wallick, *J. Am. Chem. Soc.*, 1988, **110**, 2026; (d) H. G. Jang, D. D. Cox and L. Que, Jr, *J. Am. Chem. Soc.*, 1991, **113**, 9200.
- 11 (a) R. H. Heistand, II, A. L. Roe and L. Que, Jr, *Inorg. Chem.*, 1982, **21**, 676; (b) R. H. Heistand, II, R. B. Lauffer, E. Fikrig and L. Que, Jr, *J. Am. Chem. Soc.*, 1982, **104**, 2789.
- 12 H. Fuji and Y. Funahashi, *Angew. Chem., Int. Ed.*, 2002, **41**, 3638.
- 13 (a) T. Funabiki, T. Yamazaki, A. Fukui, T. Tanaka and S. Yoshida, *Angew. Chem., Int. Ed.*, 1998, **37**, 513; (b) T. Funabiki, A. Mizoguchi, T. Sugimoto, S. Tada, M. Tsuji, H. Sakamoto and S. Yoshida, *J. Am. Chem. Soc.*, 1986, **108**, 2921.
- 14 (a) R. Viswanathan, M. Palaniandavar, T. Balasubramanian and P. T. Muthiah, *Inorg. Chem.*, 1998, **37**, 2943; (b) M. Palaniandavar and R. Viswanathan, *Proc. Indian Acad. Sci., Chem. Sci.*, 1996, **108**, 235; (c) R. Viswanathan, M. Palaniandavar, T. Balasubramanian and P. T. Muthiah, *J. Chem. Soc., Dalton Trans.*, 1996, 2519; (d) R. Viswanathan and M. Palaniandavar, *J. Chem. Soc., Dalton Trans.*, 1995, 1259.
- 15 M. Pascaly, M. Duda, A. Rompel, B. H. Sift, W. M. Klauke and B. Krebs, *Inorg. Chim. Acta*, 1999, **291**, 289.
- 16 M. Pascaly, M. Duda, F. Scweppe, K. Zurlinden, F. K. Muller and B. Krebs, *J. Chem. Soc., Dalton Trans.*, 2001, 828.
- 17 (a) P. Mialane, L. Tchertanov, F. Banse, J. Sainon and J.-J. Girerd, *Inorg. Chem.*, 2000, **39**, 2440; (b) P. Mialane, E. Anxolabèhère-Mallart, G. Blondin, A. Nivorojkine, J. Guilhem, L. Tchertanova, M. Cesario, N. Ravi, E. Bominaar, J.-J. Girerd and E. Münck, *Inorg. Chim. Acta*, 1997, **263**, 367; (c) N. Raffard, R. Carina, A. J. Simaan, J. Sainon, E. Riviere, L. Tchertanov, S. Bourcier, G. Bouchoux, M. Delroisse, F. Banse and J. J. Girerd, *Eur. J. Inorg. Chem.*, 2001, 2249.
- 18 W. O. Koch, V. Schünemann, M. Gerdan, A. X. Trautwein and H. J. Krüger, *Chem.–Eur. J.*, 1998, **4**, 1255.
- 19 R. Yamahara, S. Ogo, Y. Watanabe, T. Funabiki, K. Jitsukawa, H. Masuda and H. Einaga, *Inorg. Chim. Acta*, 2000, **300–302**, 587.
- 20 (a) M. Velusamy, M. Palaniandavar, R. Srinivasagopalan and G. U. Kulkarni, *Inorg. Chem.*, 2003, **42**, 8283; (b) M. Velusamy, R. Mayilmurugan and M. Palaniandavar, *Inorg. Chem.*, 2004, **43**, 6284; (c) M. Palaniandavar and R. Mayilmurugan, *C. R. Chim.*, 2007, **10**, 366; (d) M. Palaniandavar, M. Velusamy and R. Mayilmurugan, *J. Chem. Sci.*, 2006, **118**, 601.
- 21 (a) M. Velusamy, R. Mayil Murugan and M. Palaniandavar, *J. Inorg. Biochem.*, 2005, **99**, 1032; (b) T. Dhanalakshmi, T. Bhuvanaeshwari and M. Palaniandavar, *J. Inorg. Biochem.*, 2006, **100**, 1527.
- 22 T. Funabiki, H. Sakamoto, S. Yoshida and K. Tarama, *J. Chem. Soc., Chem. Commun.*, 1986, 1699.
- 23 A. Dei, D. Gatteschi and L. Pardi, *Inorg. Chem.*, 1993, **32**, 1389.
- 24 M. Ito and L. Que, Jr, *Angew. Chem., Int. Ed. Engl.*, 1997, **36**, 1342.
- 25 (a) T. D. H. Bugg, G. Lin and G. Reid, *J. Am. Chem. Soc.*, 2001, **123**, 5030; (b) G. Lin, G. Reid and T. D. H. Bugg, *Chem. Commun.*, 2000, 1119.
- 26 S. Yoon, H. J. Lee and H. G. Jang, *Bull. Korean Chem. Soc.*, 2000, **21**, 923.
- 27 T. Oghihara, S. Hikichi, M. Akita and M. Moro-Oka, *Inorg. Chem.*, 1998, **37**, 2614.
- 28 D. H. Jo and L. Que, Jr, *Angew. Chem., Int. Ed.*, 2000, **39**, 4284.
- 29 S. Ogo, R. Yamahara, T. Funabiki, H. Masuda and Y. Watanabe, *Chem. Lett.*, 2001, 1062.
- 30 K. Sundaravel, T. Dhanalakshmi, E. Suresh and M. Palaniandavar, *Dalton Trans.*, 2008, 7012.
- 31 K. Viswaganesan, R. Mayil Murugan, E. Suresh and M. Palaniandavar, *Inorg. Chem.*, 2007, **46**, 10294.
- 32 P. C. A. Bruijninx, M. Lutz, A. L. Spek, W. R. Hagen, B. M. Weckhuysen, G. Koten and R. J. M. Klein Gebbink, *J. Am. Chem. Soc.*, 2007, **129**, 2275.
- 33 R. Mayilmurugan, E. Suresh and M. Palaniandavar, *Inorg. Chem.*, 2007, **46**, 6038.
- 34 R. Mayilmurugan, H. Stoeckli-Evans and M. Palaniandavar, *Inorg. Chem.*, 2008, **47**, 6645.
- 35 S. Trofimenko, J. C. Calabrese, P. J. Domaille and J. S. Thompson, *Inorg. Chem.*, 1989, **28**, 1091.
- 36 D. L. Reger, T. C. Grattan, K. J. Brown, C. A. Little, J. J. Lamba, A. L. Rheingold and R. D. Sommer, *J. Organomet. Chem.*, 2000, **607**, 120.
- 37 (a) M. Duda, M. Pascaly and B. Krebs, *Chem. Commun.*, 1997, 835; (b) J.-Y. Xu, J. Astner, O. Walter, F. W. Heinemann, D. Schnieders, M. Merkel and B. Krebs, *Eur. J. Inorg. Chem.*, 2006, 1601.
- 38 L. S. White, P. V. Nilsson, L. H. Pignolet and L. Que, Jr, *J. Am. Chem. Soc.*, 1984, **106**, 8312.
- 39 (a) M. W. Vetting, Ph.D. Thesis, University of Minnesota, 2002; (b) F. H. Vaillancourt, C. J. Barbosa, T. G. Spiro, J. T. Bolin, M. W. Blades, R. F. B. Turner and L. D. Eltis, *J. Am. Chem. Soc.*, 2002, **124**, 2485; (c) N. Sato, Y. Urugami, T. Nishizaki, Y. Takahashi, G. Sazaki, K. Sugimoto, T. Nonaka, E. Masai, M. Fukuda and T. Senda, *J. Mol. Biol.*, 2002, **321**, 621.
- 40 E. G. Kovaleva and J. D. Lipscomb, *Science*, 2007, **316**, 453.
- 41 (a) D. T. Sawyer, A. Sobkowiak and J. I. Roberts, Jr, *Electrochemistry for Chemists*, Wiley-Interscience, New York, 2nd edn, 1995, p. 136; (b) E. J. Nanni, M. D. Stallings and D. T. Sawyer, *J. Am. Chem. Soc.*, 1980, **102**, 4481.
- 42 *SMART & SAINT Software Reference manuals, version 5.0*, Bruker AXS Inc., Madison, WI, 1998.
- 43 G. M. Sheldrick, *SADABS software for empirical absorption correction*, University of Göttingen, Germany, 2000.
- 44 *SHELXTL Reference Manual, version 5.1*, Bruker AXS Inc., Madison, WI, 1998.